Looking through the mirror: Optical microcavity-mirror image photonic interaction

Lei Shi,[1,2] E. Xifré-Pérez,[3] F. J. García de Abajo,[4] and F. Meseguer [1,2,*]

[1] *Centro de Tecnologías Físicas, Unidad Asociada ICMM/CSIC-UPV, Universidad Politécnica de Valencia Av. Los Naranjos s/n, Valencia, 46022, Spain*
[2]*Instituto de Ciencia de Materiales de Madrid CSIC, Sor Juana Ines de la Cruz sn, Cantoblanco, Madrid, Spain*
[3]*ICFO-Institut de Ciencies Fotoniques, Mediterranean Technology Park, 08860 Castelldefels (Barcelona), Spain*
[4] *IQFR- CSIC, Serrano 119, 28006 Madrid, Spain*
[*]*fmese@fis.upv.es*

Abstract: Although science fiction literature and art portray extraordinary stories of people interacting with their images behind a mirror, we know that they are not real and belong to the realm of fantasy. However, it is well known that charges or magnets near a good electrical conductor experience real attractive or repulsive forces, respectively, originating in the interaction with their images. Here, we show strong interaction between an optical microcavity and its image under external illumination. Specifically, we use silicon nanospheres whose high refractive index makes well-defined optical resonances feasible. The strong interaction produces attractive and repulsive forces depending on incident wavelength, cavity-metal separation and resonance mode symmetry. These intense repulsive photonic forces warrant a new kind of optical levitation that allows us to accurately manipulate small particles, with important consequences for microscopy, optical sensing and control of light by light at the nanoscale.

OCIS codes: (350.4855) Optical tweezers or optical manipulation; (160.3918) Metamaterials; (290.4020) Mie theory.

References and links

1. J. D. Jackson, *Classical Electrodynamics* (John Wiley & Sons, Inc, 1962).
2. E. H. Brandt, "Levitation in physics," Science **243**(4889), 349–355 (1989).
3. I. V. Lindell, E. Alanen, and K. Mannersalo, "Exact image method for impedance computation of antennas above the ground," IEEE Trans. Antenn. Propag. **AP-33**, 937–945 (1984).
4. R. Fenollosa, F. Meseguer, and M. Tymczenko, "Silicon colloids: from microcavities to photonic sponges," Adv. Mater. (Deerfield Beach Fla.) **20**(1), 95–98 (2008).
5. E. Xifré-Pérez, R. Fenollosa, and F. Meseguer, "Low order modes in microcavities based on silicon colloids," Opt. Express **19**(4), 3455–3463 (2011).
6. E. Xifré-Pérez, F. J. García de Abajo, R. Fenollosa, and F. Meseguer, "Photonic binding in silicon-colloid microcavities," Phys. Rev. Lett. **103**(10), 103902 (2009).
7. A. García-Etxarri, R. Gómez-Medina, L. S. Froufe-Pérez, C. López, L. Chantada, F. Scheffold, J. Aizpurua, M. Nieto-Vesperinas, and J. J. Sáenz, "Strong magnetic response of submicron silicon particles in the infrared," Opt. Express **19**(6), 4815–4826 (2011).
8. N. Engheta, "Circuits with light at nanoscales: optical nanocircuits inspired by metamaterials," Science **317**(5845), 1698–1702 (2007).
9. R. Merlin, "Metamaterials and the Landau-Lifshitz permeability argument: large permittivity begets high-frequency magnetism," Proc. Natl. Acad. Sci. U.S.A. **106**(6), 1693–1698 (2009).
10. C. M. Soukoulis, M. Kafesaki, and E. N. Economou, "Negative index materials: new frontiers in optics," Adv. Mater. (Deerfield Beach Fla.) **18**(15), 1941–1952 (2006).
11. D. R. Smith, J. B. Pendry, and M. C. K. Wiltshire, "Metamaterials and negative refractive index," Science **305**(5685), 788–792 (2004).
12. M. Burresi, D. van Oosten, T. Kampfrath, H. Schoenmaker, R. Heideman, A. Leinse, and L. Kuipers, "Probing the magnetic field of light at optical frequencies," Science **326**(5952), 550–553 (2009).
13. A. Ashkin, "Acceleration and trapping of particles by radiation pressure," Phys. Rev. Lett. **24**(4), 156–159 (1970).
14. A. Ashkin and J. M. Dziedzic, "Observation of resonances in the radiation pressure on dielectric spheres," Phys. Rev. Lett. **38**(23), 1351–1354 (1977).

#164605 - $15.00 USD Received 13 Mar 2012; revised 4 Apr 2012; accepted 5 Apr 2012; published 1 May 2012

15. A. Ashkin and J. M. Dziedzic, "Optical trapping and manipulation of viruses and bacteria," Science **235**(4795), 1517–1520 (1987).
16. K. Dholakia, P. Reece, and M. Gu, "Optical micromanipulation," Chem. Soc. Rev. **37**(1), 42–55 (2007).
17. D. G. Grier, "A revolution in optical manipulation," Nature **424**(6950), 21–27 (2003).
18. F. M. Fazal and S. M. Block, "Optical tweezers study life under tension," Nat. Photonics **5**(6), 318–321 (2011).
19. M. Righini, A. S. Zelenina, C. Girard, and R. Quidant, "Parallel and selective trapping in a patterned plasmonic landscape," Nat. Phys. **3**(7), 477–480 (2007).
20. M. L. Juan, M. Righini, and R. Quidant, "Plasmon nano-optical tweezers," Nat. Photonics **5**(6), 349–356 (2011).
21. R. Quidant and C. Girard, "Surface-plasmon-based optical manipulation," Laser Photon. Rev. **2**(1-2), 47–57 (2008).
22. M. Righini, G. Volpe, C. Girard, D. Petrov, and R. Quidant, "Surface plasmon optical tweezers: tunable optical manipulation in the femtonewton range," Phys. Rev. Lett. **100**(18), 186804 (2008).
23. G. Volpe, R. Quidant, G. Badenes, and D. Petrov, "Surface plasmon radiation forces," Phys. Rev. Lett. **96**(23), 238101 (2006).
24. M. Righini, P. Ghenuche, S. Cherukulappurath, V. Myroshnychenko, F. J. García de Abajo, and R. Quidant, "Nano-optical trapping of Rayleigh particles and Escherichia coli bacteria with resonant optical antennas," Nano Lett. **9**(10), 3387–3391 (2009).
25. P. W. Barber and S. C. Hill, *Lights Scattering by Particles: Computational Methods* (World Scientific, Singapore, 1990).
26. T. Sannomiya and C. Hafner, "Multiple multipole program modelling for nano plasmonic sensors," J. Comput. Theor. Nanoscience **7**(8), 1587–1595 (2010).
27. L. Novotny, D. W. Pohl, and B. Hecht, "Scanning near-field optical probe with ultrasmall spot size," Opt. Lett. **20**(9), 970–972 (1995).
28. F. J. García de Abajo, "Multiple scattering of radiation in clusters of dielectrics," Phys. Rev. B **60**(8), 6086–6102 (1999).
29. E. Palik, *Handbook of Optical Constants of Solids* (Academic Press, New York, 1985).
30. R. Zhao, P. Tassin, T. Koschny, and C. M. Soukoulis, "Optical forces in nanowire pairs and metamaterials," Opt. Express **18**(25), 25665–25676 (2010).
31. X. Yang, Y. Liu, R. F. Oulton, X. Yin, and X. Zhang, "Optical forces in hybrid plasmonic waveguides," Nano Lett. **11**(2), 321–328 (2011).
32. F. J. García de Abajo, "Momentum transfer to small particles by passing electron beams," Phys. Rev. B **70**(11), 115422 (2004).
33. K. M. Hurst, C. B. Roberts, and W. R. Ashurst, "A gas-expanded liquid nanoparticle deposition technique for reducing the adhesion of silicon microstructures," Nanotechnology **20**(18), 185303 (2009).
34. J. N. Israelachvili, *Intermolecular and Surface Forces* (Academic, London, 1992).
35. A_{11} equal to 31×10^{-20} J; A_{22} equal to 6.5×10^{-20}; A_{33} equal to 4×10^{-20}.

1. Introduction

The theory of image charges offers a useful method for solving the electric and magnetic field distributions of either a charge or a magnet near the flat surface of a perfect electric conductor (PEC) [1]. In particular, the field distribution for a charge is obtained by replacing the conductor by a fictitious charge placed at the mirror image of the real charge, but with opposite sign (Fig. 1(a)). For a magnet near a PEC surface, the mirror magnet has a magnetization vector that is just the specular reflection of the magnetization vector produced by the real source (Fig. 1(b)). We therefore conclude that the force between a charge and a PEC surface is always attractive, whereas the force between a magnet and a PEC surface is always repulsive. This simple analysis finds application to electrostatic adsorption and magnetic levitation [2].

Here, we show that the method of charge and magnet images can be extended for understanding the effect of flat metallic surfaces on the modes of neighbouring dielectric microcavities, and theoretically show the application of these concepts to a new form of optical levitation. We follow a procedure similar to the simulation of electromagnetic (EM) modes in resonant antenna near earth ground [3]. Specifically, we use silicon colloids [4] as high-refractive-index nanometre-sized spherical microcavities because they display well-defined, sharp Mie resonances with huge scattering cross-sections [5, 6]. The microcavity modes can be envisaged as electric and magnetic oscillating multipoles. The presence of a flat metallic surface induces mirror EM multipole images. In particular, the electric-dipole (ED) mode parallel to the surface is the easiest to understand: in an electrostatic picture, the metallic surface induces an imaginary ED with antiparallel dipole moment (see Fig. 1(c)), and consequently, the microcavity undergoes attraction towards the conductor. In contrast, a parallel magnetic dipole (MD) induces a mirror parallel magnetic dipole, which results in a

#164605 - $15.00 USD Received 13 Mar 2012; revised 4 Apr 2012; accepted 5 Apr 2012; published 1 May 2012

repulsive photonic force (see Fig. 1(c)). Generally speaking, multipolar optical modes in microcavities near good conductors induce attractive or repulsive forces depending on the type of resonance that is involved. The net photonic force acting on the microcavity under illumination by a laser impinging perpendicularly to the metal surface emerges from the balance between attractive and repulsive forces acting on it. The photonic force is stronger for modes producing larger scattering cross-section (e.g., modes in cavities with high refractive index such as our silicon microspheres). However, magnetic (TM) and electric (TE) resonances usually are close in wavelength, and consequently, attractive and repulsive forces tend to cancel out, except for low-order modes, which tend to be well separated (see Fig. 2). More precisely, magnetic-like photonic forces are dominant for low-order TM modes with strong scattering (e.g., the fundamental TM mode b11, see Fig. 2) and well apart from TE modes. TM modes also exhibit large magnetic response [7]. Here we demonstrate a dominant magnetic repulsive force over the electrical attractive force in silicon nanospheres when the external light is tuned near the b11 resonance. This repulsive photonic force is larger than other competing forces such as van der Waals (vdW) attraction and Brownian motion.

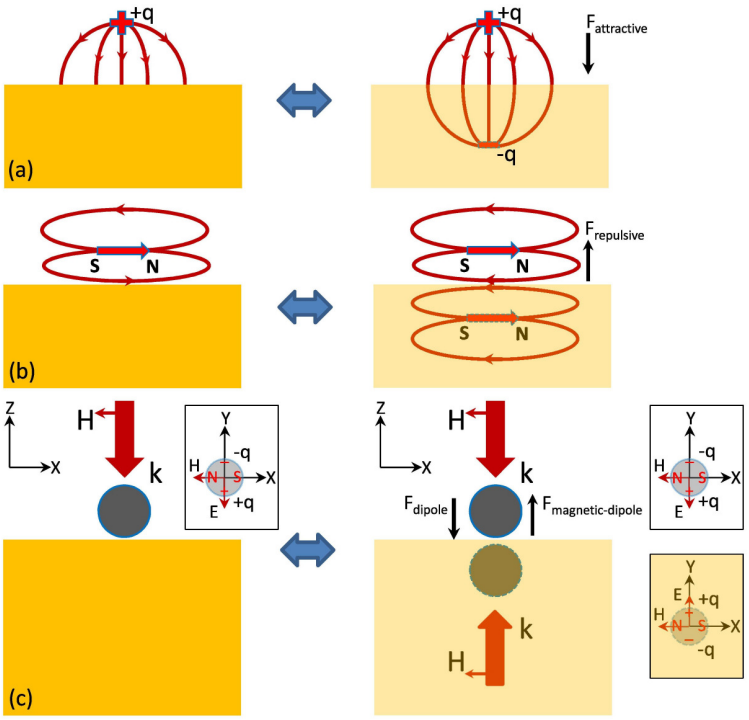

Fig. 1. **Schematic view of the mirror image method.** (a) Schematic view of the mirror image method for a single electrical charge. The direction of the force between the charge and the metal is shown in left panel. (b) Schematic view of the mirror image method for a magnetic dipole. The direction of the force on magnet is shown in left panel. (c) Schematic view of the mirror image method applied to a microcavity (grey sphere) near a metallic conductor. The thick dark red arrow indicates the incident EM wave. The thin dark red arrow indicates the (**H**) field direction of the incident EM wave. The upper inset shows the directions of the incident (**E**) and (**H**) fields in the x-y plane (the planar surface is at z = 0). The lower inset shows the direction of (**E**) and (**H**) fields in the image, along with the corresponding electric and magnetic image dipoles. We also show the direction of the forces acting on the optical cavity originating in electric and magnetic dipoles.

Magnetism at optical frequencies has recently been achieved through elaborate metamaterials designs [8–11], and even direct evidence of the resulting magnetic field has been reported using an artificial magnetic atom attached to a probing tip [12]. In this context, our silicon nanospheres constitute a new class of magnetic atoms, capable of amplifying the

#164605 - $15.00 USD Received 13 Mar 2012; revised 4 Apr 2012; accepted 5 Apr 2012; published 1 May 2012

magnetic component of the EM waves at optical frequencies, which in turns produces repulsive forces near a metal surface.

Photonic forces are extensively used in optical tweezers [13–15] for manipulating microparticles [16–18]. Recently, plasmons have been realized to produce intense gradient forces capable of trapping small nanoparticles [19–24]. In these studies, low-refractive-index dielectrics are used, producing relatively weak scattering [25]. This is in contrast to our high-index nanospheres, from which we derive completely new phenomena under external illumination for wavelengths in resonance with low-order magnetic and electric optical modes near a metallic film.

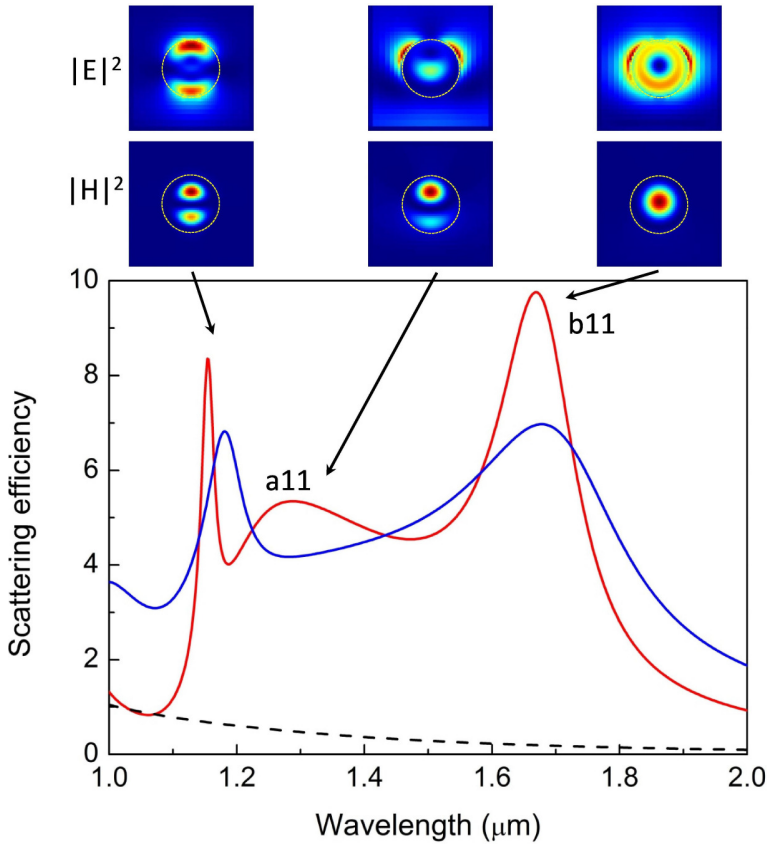

Fig. 2. Scattering efficiency of a single silicon sphere, immersed in vacuum (red line) and water (blue line), as a function of light wavelength. The scattering efficiency of single PS sphere in vacuum (black dash line) is also plotted. The E and H field intensity distribution of silicon sphere in vacuum for some of the Mie modes are also shown above. The radius of both silicon and PS spheres is 230 nm.

In this work, we show that EM field distribution of the low-order modes of a spherical optical microcavity near a metallic surface under external laser irradiation is identical to the EM field of a particle dimer in which each particle is illuminated with counter-propagating laser beams, as deduced from the mirror image method discussed above. We also report strong repulsive photonic forces four orders of magnitude larger than the particle weight ($F = mg = 1.2\times10^{-3}$ pN) over a broad range of laser wavelengths. Importantly, the optical force acting on a silicon nanosphere can be tuned from repulsive to attractive and vice versa by selecting either the light wavelength or the gap between the sphere and the metal.

#164605 - $15.00 USD Received 13 Mar 2012; revised 4 Apr 2012; accepted 5 Apr 2012; published 1 May 2012

2. Numerical methods

We calculate both EM fields and optical forces through two methods; a) by rigorously solving Maxwell's equations using a highly convergent multiple-scattering method based upon a multipolar expansion of the fields near the sphere and an expansion in plane waves elsewhere, including reflection at the planar metal surface (MESME). This is similar to previous approaches based on the multiple multipole method [26, 27] and specific implementations for aggregates of up to thousands of spherical particles [28]; b) by finite difference time domain simulation (FDTD) calculation using the public software (Lumerical FDTD Solutions). The results from both methods are in full agreement with each other. The dielectric constant of Au is taken from Ref [29], while we assume a frequency independent refractive index of 3.5 and 1.6 for silicon and polystyrene (PS), respectively. The radius of the silicon sphere is set to 230 nm, so that the fundamental optical modes appear in the near-infrared (NIR) region. The optical force is obtained upon integration of the Maxwell stress tensor [30, 31], which results in an analytical formula in terms of the multipolar field components near the sphere [32]. A plane EM wave at normal incidence with 10 mW/μm^2 is presumed. However, due to the small size of the microcavity only a tiny power fraction (1.6 mW) is directly impinging on the sphere.

3. Results and discussion

We start by inspecting the EM field distribution in the microcavity placed near a PEC surface, as shown schematically in the insets of Fig. 3(b). Because of the high refractive index of silicon, a sphere as small as 0.46 μm is capable of supporting well-defined low-order Mie resonance modes (as shown in Fig. 2). The lowest-order Mie mode resonances (b11 and a11 in Fig. 2) correspond to transverse magnetic (TM) and transverse electric (TE) modes. We have plotted the EM field distribution for two wavelengths (λ = 1434 nm and λ = 1744 nm) at which TM and TE are dominant (see below). The upper plots of Fig. 3(a) (TM dipole, TMD), show the distribution of Ex, Ez and Hy fields at 1434 nm, where the TM mode b11 is dominant. In particular, Ex shows a typical dipole feature, which demonstrates that the incident light induces an electric dipole resonance. Interestingly, Ez shows strong enhancement in the gap region, which illustrates the strong coupling existing between the sphere and the metal surface. The Hy component indicates that the incident light also induces a very strong magnetic dipole resonance in the silicon sphere. Both modes contribute to the scattering cross-section but compete with each other to produce a net photonic force (see Fig. 3(b)). The lower plots of Fig. 3(a) show the EM field at a wavelength of 1744 nm, for which the TE mode becomes dominant (TE dipole, TED). Figure 3(c) shows the EM field distribution at the same wavelengths as in Fig. 3(a), but for the case of a dimer consisting of two identical microcavities located symmetrically with respect the (now absent) metal interface and illuminated by counter-propagating laser beams, phase-shifted by π with respect to each other, as suggested by direct application of the mirror image method. The EM fields in both microcavities at λ = 1434 nm (upper plots) and λ = 1744 nm (lower plots) have a plane of symmetry at the planar surface, while the fields in the upper semi-space are identical to those of Fig. 3(a). Comparison between the full calculation and the image method for different modes and parameters thus results in identical field distributions. Therefore, the image method can be extended to electrodynamics when microcavities near a perfect conductor are considered.

#164605 - $15.00 USD Received 13 Mar 2012; revised 4 Apr 2012; accepted 5 Apr 2012; published 1 May 2012

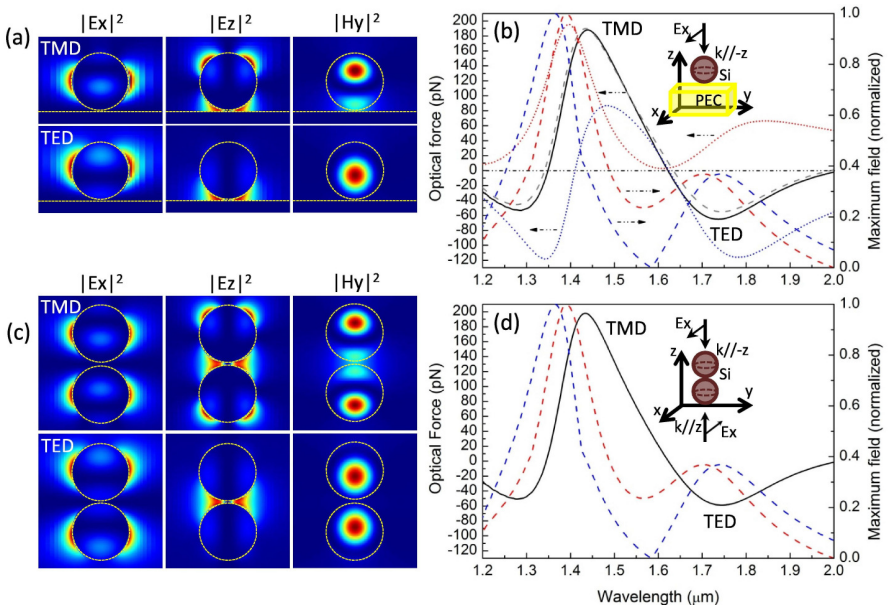

Fig. 3. **Optical force on a silicon nanosphere near a PEC surface.** (a) Distribution of E_x, E_z and H_y field components within the x-z plane for a silicon nanosphere near a PEC surface at wavelengths of 1434 nm (TMD, upper panels) and 1744 nm (TED, lower panels). (b) Optical force along the z direction (black solid curve obtained from FDTD, grey dash line curve obtained from MESME, red dotted curve obtained from integration only the magnetic part of the Maxwell tensor, blue dotted curve obtained from integration of the electric part of Maxwell tensor [30, 31]; left axis) and maximum of the E_z and H_y fields (blue and red dashed curves, respectively; right axis) acting on a silicon sphere separated by a 10 nm gap from a PEC surface as a function of wavelength. The sphere radius is 230 nm. The light intensity is 10mW/μm^2. (c) E_x, E_z and H_y field distributions in the x-z plane for two neighbouring spheres at 1434 nm (TMD, upper panels) and 1744 nm (TED, lower panels). (d) Optical force along the z direction (black solid curve; left axis) and maximum E_z and H_y fields (blue and red dashed curves, respectively; right axis) for two spheres separately irradiated by counter-propagating incident light with π phase difference as a function of wavelength. The sphere size and light intensity is the same as in (a). The separation between the two spheres is 20 nm.

Now, we examine the resulting optical forces. The black solid curve (FDTD results) and the grey dash curve (MESME results) in the Fig. 3(b) show the optical force acting on a silicon sphere near a PEC surface (gap equal to 10 nm) as a function of incident wavelength. Positive values correspond to repulsive forces. A strong repulsive optical force opposite to the laser wave vector direction emerges in the region between 1400 nm and 1600 nm. Figure 3(d) shows the photonic force acting on two spheres irradiated by counter-propagating EM beams as the mirror image method states. The beams have a π phase difference between them. The photonic force acting on the upper sphere is identical to the one calculated in Fig. 3(b). It clearly proves that the strong photonic force of silicon sphere on PEC originates from the strong photonic interaction between silicon sphere and its mirror image. Red and blue dashed curves in Figs. 3(b) and 3(d) show the maximum fields Hy (responsible for the repulsive force) and Ez (responsible for the attractive force), indicating that the strong repulsive force dominated by the magnetic resonance. It is very difficult separating the electric and magnetic dipole contributions because strong magnetic resonances induce strong displacement E fields. However, in order to deeper understand the optical process we have separated both the electric and magnetic field component of Maxwell tensor (blue and red dotted curves shown in Fig. 3(b)), and we have obtained similar results.

#164605 - $15.00 USD Received 13 Mar 2012; revised 4 Apr 2012; accepted 5 Apr 2012; published 1 May 2012

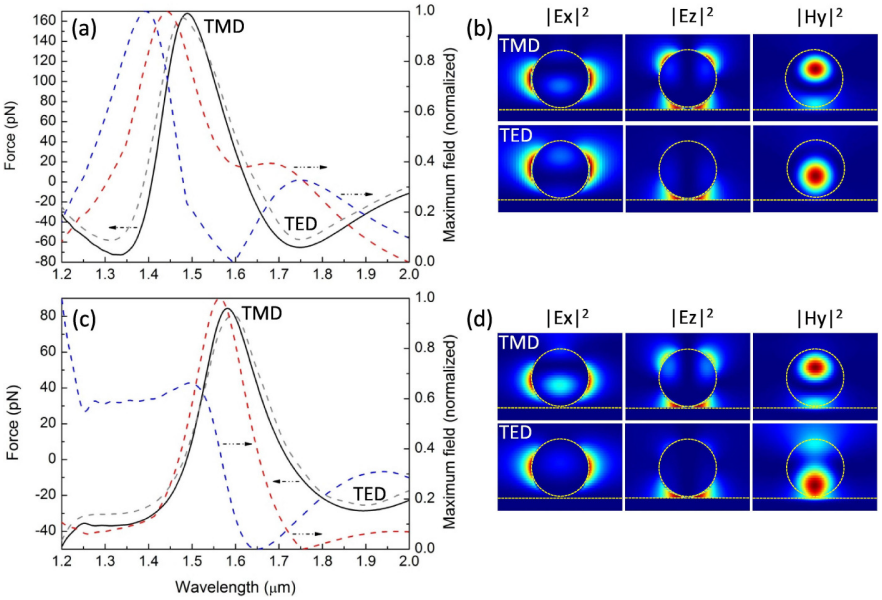

Fig. 4. **Optical force on a silicon nanosphere near a real metal.** (a) Optical force along the z direction (black solid curve obtained from FDTD, grey dash line curve obtained from MESME; left axis) and maximum E_z and H_y fields (blue and red dashed curves, respectively; right axis) for a silicon sphere in vacuum separated by a 10 nm gap from a gold surface as a function of wavelength. The sphere radius is 230 nm. The light intensity is 10 mW/μm^2. (b) E_x, E_z and H_y field distributions in the x-z plane for a silicon sphere in vacuum at wavelengths of 1490 nm (TMD, upper panels) and 1750 nm (TED, lower panels). (c) Same as (a) for a silicon sphere suspended in water near a gold surface. (d) E_x, E_z and H_y field distributions in the x-z plane for a sphere in water near a gold surface at 1582 nm (TMD, upper panels) and 1894 nm (TED, lower panels).

Figure 4 shows results for a real gold mirror with the microcavity suspended in either vacuum (Figs. 4(a) and 4(b)) or water (Figs. 4(c) and 4(d)). The black solid curve (FDTD results) and the grey dash curve (MESME results) in Fig. 4(a) show the optical force on the silicon sphere as a function of incident wavelength. Clearly, a strong repulsive optical force appears in the wavelength between 1408 nm and 1624 nm. At 1490 nm, the repulsive force is about five orders of magnitude larger than the weight of the silicon sphere itself. Because most optical tweezers work in liquid phase, Figs. 4(c) and 4(d) show a more realistic scenario, in which the metal is gold and the spheres are suspended in water. The results are similar to vacuum or air. The repulsive force maximum appears slightly red shifted because of the high refractive index of water. However, the photonic force with water is about half the value of that appearing with vacuum or air. From the maxima of the Ez (blue dash curve in Fig. 4(a), 4(c)) and Hy (red dash curve in Fig. 4(a), 4(c)) fields, it is again clear that this strong repulsive force dominated by the magnetic resonance. For a low-refractive-index cavity (e.g., a PS sphere) of the same size as the silicon microspheres, Mie modes are much less well defined (see Fig. 2), and as expected, only very tiny photonic forces are observed (not shown).

#164605 - $15.00 USD Received 13 Mar 2012; revised 4 Apr 2012; accepted 5 Apr 2012; published 1 May 2012

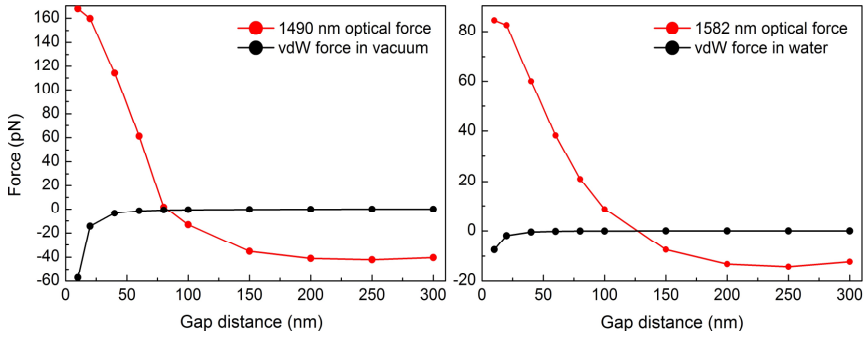

Fig. 5. **Optical force in different media as a function of sphere-metal separation and sphere dynamic motion.** (a) Optical force (red curve) along the z direction for a silicon sphere in vacuum near a gold surface as a function of silicon-gold gap distance. The wavelength of incident light is 1490 nm. The radius of the sphere is 230 nm. The light intensity is 10 mW/μm^2. The van der Waals (vdW) force (black curve) is shown for comparison (see main text for details). (b) Same as (a) with silicon sphere in water near a gold surface. The laser wavelength is 1582 nm in all cases.

Finally, we estimate the degree of detectability of the forces under consideration calculating them as a function of the gap between the sphere and the mirror. We plot in the Fig. 5 the photonic repulsion as a function of gap distance. We use two different wavelength, λ = 1490 nm, and λ = 1580 nm, for vacuum and water medium, respectively. The vdW force acting on the sphere on surface can be approximated as [33], F = Ar/(6s^2), where A is the Hamaker constant, r is the sphere radius, and s is the distance between the sphere and the surface. The overall Hamaker constant is approximated as $A \approx (\sqrt{A_{11}} - \sqrt{A_{33}})(\sqrt{A_{22}} - \sqrt{A_{33}})$ [33, 34], where A_{11}, A_{22} and A_{33} are the individual Hamaker constants for gold, silicon and the vacuum or water medium, respectively [33–35]. From the results of Fig. 5, we see the vdW force is significantly weaker than the optical force (up to 2 orders of magnitude). Down to very small separations ~10 nm, the vdW force is more than twice smaller than the optical repulsive force for a laser intensity of 10 mW/μm^2. Even at perfectly reachable lower intensity ~1 mW/μm^2, photonic repulsion is still stronger than vdW in water case. Additionally, Brownian force is completely negligible at room temperature (10 fN). From Fig. 5 we deduce that the particle is subject to either repulsive or attractive forces depending on the gap distance. Therefore, particles of 460 nm near a gold mirror and illuminated with an external laser of the appropriate wavelength should undergo oscillatory motion around an equilibrium position of zero total force. With the particle suspended in water, friction force should dampen these oscillations and lead to stable levitation of the particle.

4. Conclusion

In conclusion, we have shown that the mirror image method can be extended to deal with the optical modes of a silicon microcavity excited with a laser beam and placed near a good conductor mirror, provided a proper treatment of the image is made by exciting the image cavity with the specularly reflected external light beam. The excited optical modes of the cavity strongly interact with its image beneath the metal surface, which results in attractive or repulsive forces, depending on the symmetry of the cavity modes. The sign of the force is repulsive (attractive) when the resonant mode is TM dominant (TE dominant). Remarkably, the optical force is detectable because it is much larger than the vdW force or the Brownian force. Our results have important implications for the optical manipulation of nanoparticles, which can then be used as probes to perform subwavelength microscopy. The combination of two lasers tuned to repulsive and attractive modes of the cavity, respectively, should allow exerting full control over the position of the particle by changing the ratio between the intensities of the two lasers. Additionally, the particles can be decorated with biomarkers capable of attaching to specific biomolecules. This suggests a new way of performing

#164605 - $15.00 USD Received 13 Mar 2012; revised 4 Apr 2012; accepted 5 Apr 2012; published 1 May 2012

molecule-specific biosensing, with the advantage of a high degree of spatial control over the position of the probe. In a separate direction, a trapped particle can be regarded as a switch which interacts with probing light of a colour differing from the trapping laser, thus resulting in the control of light by light. This type of switch or modulator can reach high speeds above MHz for particles trapped in air.

Acknowledgments

L. Shi thanks the financial support from the MICINN (Estancias de profesores e investigadores extranjeros en centros españoles) fellowship program. The authors acknowledge financial support from the following projects FIS2009-07812, Consolider 2007-0046 Nanolight, MAT2010-14885, the EU (NMP4-SL-2008-213669-ENSEMBLE), and the PROMETEO/2010/043.

#164605 - $15.00 USD Received 13 Mar 2012; revised 4 Apr 2012; accepted 5 Apr 2012; published 1 May 2012